Journal of Biomedical Optics

SPIEDigitalLibrary.org/jbo

Direct high-resolution label-free imaging of cellular nanostructure dynamics in living cells

Chaejeong Heo
Sohee Lee
Si Young Lee
Mun Seok Jeong
Young Hee Lee
Minah Suh

SPIE

Direct high-resolution label-free imaging of cellular nanostructure dynamics in living cells

Chaejeong Heo,[a*] Sohee Lee,[b*] Si Young Lee,[a] Mun Seok Jeong,[a] Young Hee Lee,[a] and Minah Suh[b,c]
[a]Sungkyunkwan University, IBS Center for Integrated Nanostructure Physics (CINAP), Institute for Basic Science, Sungkyunkwan Advanced Institute of Nanotechnology (SAINT), Departments of Energy Science and Physics, Suwon 440-746, Republic of Korea
[b]Sungkyunkwan University, Samsung Advanced Institute for Health Sciences and Technology (SAIHST), Suwon 440-746, Republic of Korea
[c]Sungkyunkwan University, Department of Biological Science, Suwon 440-746, Republic of Korea

Abstract. We report the application of an optical microscope equipped with a high-resolution dark-field condenser for detecting dynamic responses of cellular nanostructures in real time. Our system provides an easy-to-use technique to visualize biological specimens without any staining. This system can visualize the dynamic behavior of nanospheres and nanofibers, such as F-actin, at the leading edges of adjacent neuronal cells. We confirmed that the nanofibers imaged with this high-resolution optical microscopic technique are F-actin by using fluorescence microscopy after immunostaining the F-actin of fixed cells. Furthermore, cellular dynamics are enhanced by applying noncontact electric field stimulation through a transparent graphene electric field stimulator. High-resolution label-free optical microscopy enables the visualization of nanofiber dynamics initiated by filopodial nanofiber contacts. In conclusion, our optical microscopy system allows the visualization of nanoscale cellular dynamics under various external stimuli in real time without specific staining. [DOI: 10.1117/1.JBO.18.6.066016]

Keywords: high-resolution imaging; live cell imaging; F-actin; label-free imaging; electrical field stimulation; graphene.

Paper 12739RR received Nov. 16, 2012; revised manuscript received May 5, 2013; accepted for publication May 7, 2013; published online Jun. 24, 2013.

1 Introduction

Microscopic bioimaging systems have rapidly progressed along with advances in immunostaining methods, and these systems are being used to investigate basic mechanisms of cell proliferation and differentiation.[1,2] In addition, microscopic bioimaging is effective for studying in real-time dynamics[3–5] of living cells responding to external stimuli.[6,7] In the past, conventional optical imaging (COI) has been a popular choice for observing real-time cellular structures and dynamics simultaneously, as COI has a large field-of-view (FOV) and easy accessibility. Recently, other contrast-enhanced COI techniques have been developed, such as photonic crystal slabs microscopy[8] and reflection interference contrast microscopy.[9] However, their spatial resolution is similar to that of the conventional microscopy. As a result, these COI techniques still have difficulty in detecting nanometer-sized cytoskeletal elements, for example, F-actin, a key molecule involved in cellular dynamics.[10] Therefore, a high-resolution real-time imaging system is needed to study nanostructure dynamics.

Scanning electron microscopy (SEM), transmission electron microscopy (TEM), and atomic force microscopy (AFM) have been used to visualize, at nanoscale resolution, features of cellular morphology such as neurite outgrowth patterns in neurons,[11] intracellular structures, anatomical connectivity,[12] and actin filament networks[13] (approximately 15 nm in diameter). However, cells must be fixed before examination with either SEM or TEM, and thus, real-time study is not possible. With AFM, the cantilever tip can damage the cell surface, and the scan speed is too slow to track the rapid cell dynamics.[14,15]

Recently, super-high resolution real-time confocal microscopic techniques have been developed based on fluorescence microscopy.[16,17] First, stimulated emission depletion—4pi optical microscopy[18,19] uses fluorescent dyes for the nonlinear de-excitation.[20,21] This technique offers 100 to 150 nm axial resolution and 5.8 nm lateral resolution.[20,21] Similar techniques include stochastic optical reconstruction microscopy,[22] photoactivation localization microscopy (PALM),[23] and fluorescent PALM.[24] These techniques can resolve images ranging from tens to a few hundreds of nanometers. Nonetheless, wider use of fluorescence microscopy is prevented by the high cost of the machine and limitations involved with the use of fluorescent dyes. Fluorescent dyes[25] can immunostain specific nanostructures such as F-actin and microtubules,[13] however, cytotoxicity and photobleaching remain problematic.[26,27]

Here, we report real-time imaging of cellular dynamics using a nanoscale optical imaging (NOI) system[28] (spatial resolution: approximately 100 nm). The NOI system combines a conventional optical microscope with a high-resolution dark-field condenser and an illumination system (CytoVivia, Inc., Auburn, Alabama). NOI can image quantum dots[29] as well as the interaction and uptake of nanoparticles in cells and tissues.[30,31] In this work, we used a noncontact electric field stimulation (nEFS) in conjunction with NOI to study the neuronal cell coupling. The enhancement of cell coupling by nEFS has been reported previously.[32] We utilized the NOI system so that we could visualize

*These authors contributed equally.

Address all correspondence to: Young Hee Lee, Sungkyunkwan University, IBS Center for Integrated Nanostructure Physics (CINAP), Institute for Basic Science, Sungkyunkwan Advanced Institute of Nanotechnology (SAINT), Departments of Energy Science and Physics, Suwon 440-746, Republic of Korea. Tel: +82-31-299-6507; Fax: +82-31-299-6505; E-mail: leeyoung@skku.edu or Minah Suh, Sungkyunkwan University, Department of Biological Science, Suwon 440-746, Republic of Korea. Tel: +82-31-299-4496; Fax: +82-31-299-4506; E-mail: minahsuh@skku.edu

individual nanofiber responses without staining the cells. The combination of nEFS and NOI allowed us to view, in real time, the fast changing behavior of nanofibers (nanometer-sized F-actin) at the leading edges of living neuronal cells.

2 Results

2.1 *Nanoscale Optical Imaging of Transparent Nanospheres Under Live Cell Conditions*

The imaging system is adapted from an inverted COI system with a live cell incubation system operated at 37°C and 5% CO_2 [Fig. 1(a)]. Neuroblastoma cells (SHSY5Y) were grown in a culture dish with an *in vitro* electric field stimulator assembly (Fig. 2). The stimulator is connected to positive and negative electrodes that receive programmed signals from a pulse generator. For NOI [Fig. 1(b)], the conventional optical condenser and halogen light source of the COI system [Fig. 1(c)] were replaced by a high-resolution dark-field condenser and an illuminator (white LED, halogen, or metal halide). In NOI, the condenser was put into the culture dish with cell media and positioned at a submillimeter distance (d_{NOI}: 10 to 1000 μm) above the cells, while the condenser of the COI was positioned several centimeters (d_{COI}: 2.5 to 4 cm) from the cells. The resolution of the NOI system was demonstrated using transparent polymers that are similar to transparent cells, 100 nm standard polystyrene nanospheres (mean diameter = 97 ± 3 nm). The nanospheres were clearly seen with a large FOV using NOI [Fig. 1(d)]. Due to the Brownian motion of nanospheres in water and high-scattering effect in NOI dark-field imaging, the apparent size of the nanospheres was 469 ± 84 nm (sample number, n = 112). In contrast, with bright-field COI (the most widely used imaging technique in cell biology), the nanospheres were not visible in the phase-contrast images [Fig. 1(e)]. For direct comparison of the two systems under dark-field conditions, we viewed nanospheres using a high numerical aperture (NA = 1.2 to 1.4) in both NOI and COI (Fig. 3).

Fixed samples of nanospheres could be viewed using either technique, but visualization of mobile nanospheres in water was significantly better with NOI [Fig. 3(d)] than with COI [Fig. 3(c)].

2.2 *Label-Free NOI of F-Actin in Living Cells*

We compared NOI and COI images of identical areas of living cells [Fig. 4; low-magnification large FOVs are shown in Fig. 4(a)–4(d) and 4(i)–4(l)]. The dark-field NOI image clearly shows neural cell nanostructures that are hard to see in the COI image, including nanofiber bundles in the filopodia, intracellular microvesicles, and the nuclear membrane. NOI can better resolve detailed nanofiber structure than COI. For example, the number of visible nanofibers was greater in NOI images [Fig. 4(e)] than in COI images [Fig. 4(f)], and the fibers were longer in the NOI images. More importantly, we can use NOI to view the finer nanofibers at junctions between interacting cells [Fig. 4(m) and 4(n)]. The differing capabilities of NOI and COI to reveal the structure at the cell's contact face are shown in Fig. 4(o) and 4(p). Overall, the NOI system shows great

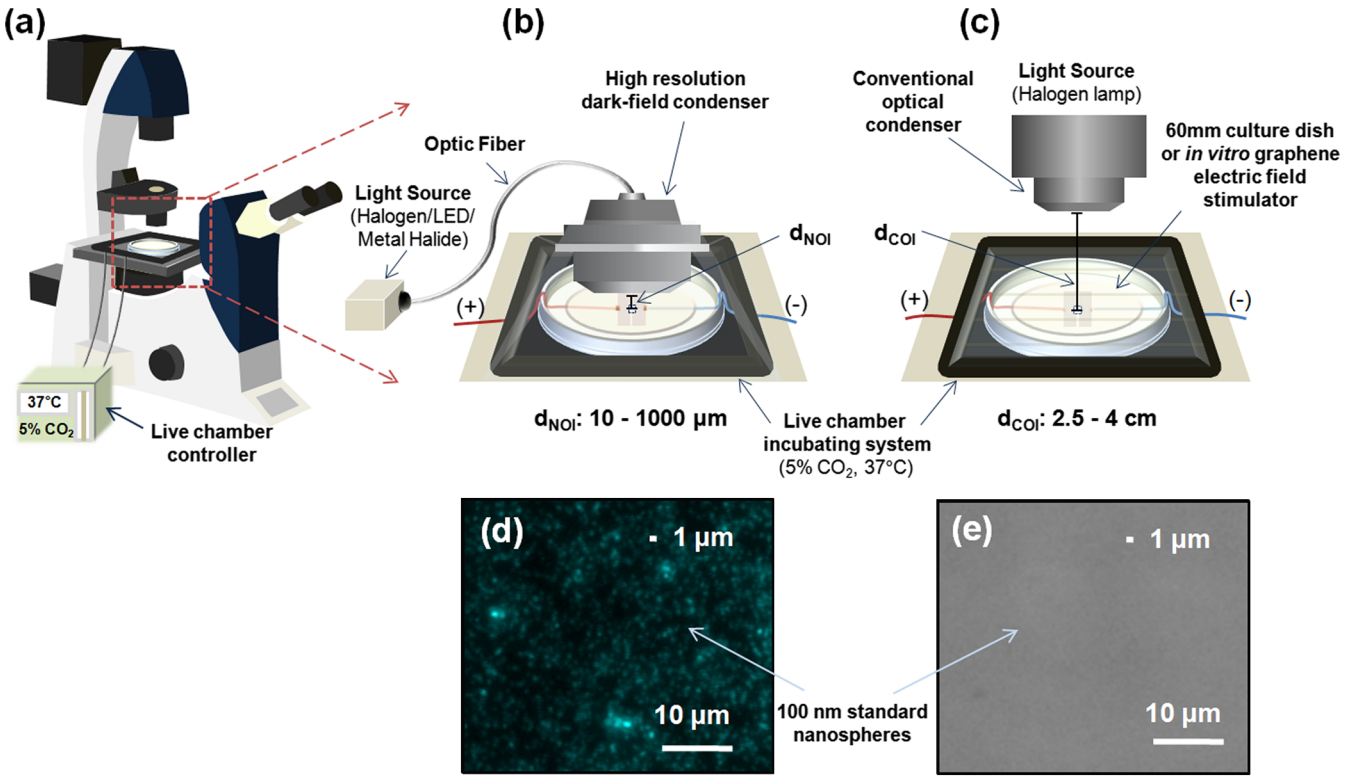

Fig. 1 Comparison of nanoscale optical imaging (NOI) and conventional optical imaging (COI) systems for real-time imaging of living cells. Illustrations of (a) a live cell imaging microscope equipped with a live-chamber controller; (b) the NOI system with a nano-optical dark-field condenser, specific illuminators, and a live-chamber system; and (c) the COI system for phase-contrast imaging with a conventional optical condenser and a live-chamber system. Images of standard polystyrene polymer nanospheres (97 ± 3 nm) observed by (d) NOI with an image size of 468.75 ± 83.85 nm and (e) COI. The distance between the high-resolution condenser and the object, d_{NOI}, was approximately 10 to 1000 μm, and the distance between the condenser and the object, d_{COI}, was approximately 2.5 to 4 cm.

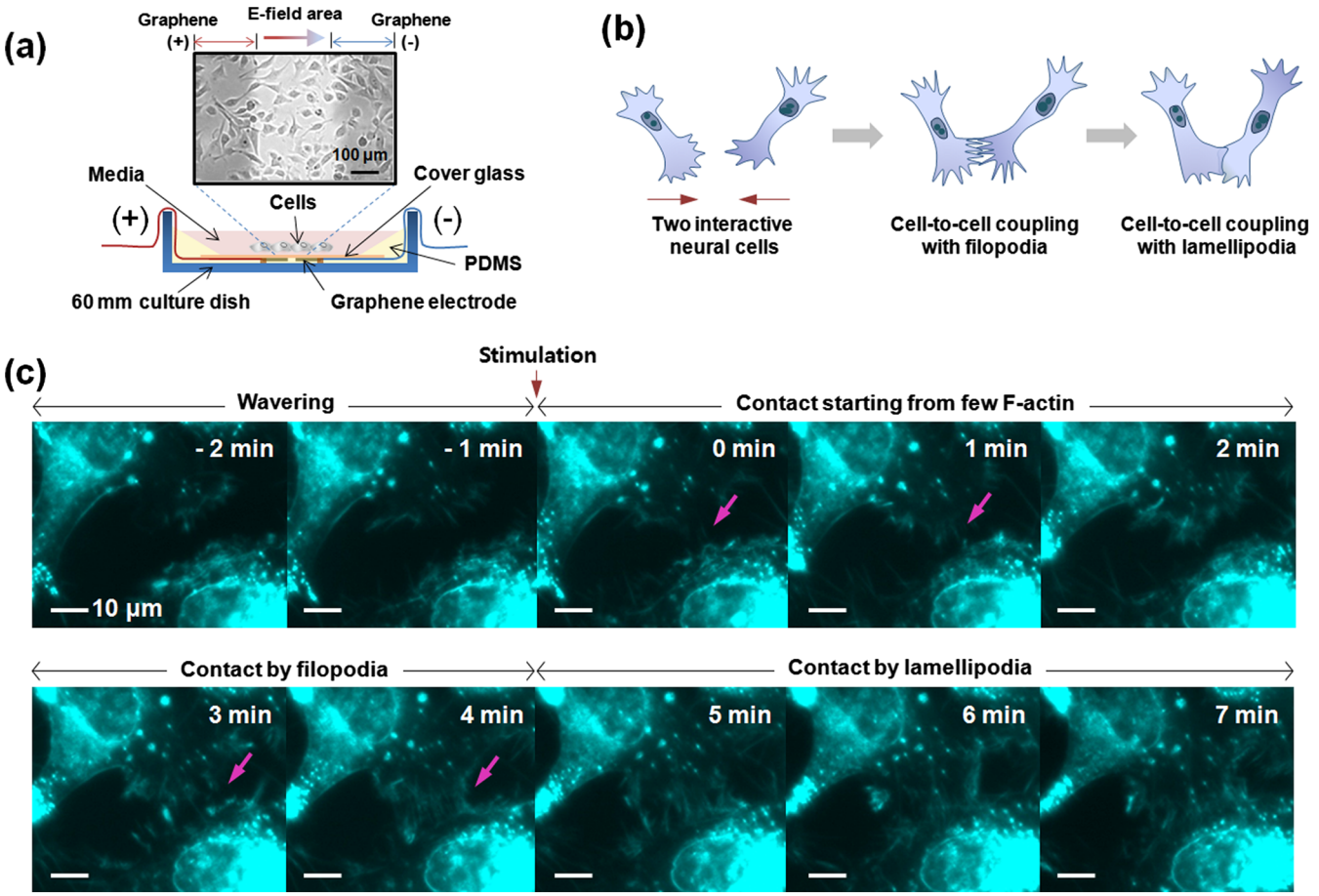

Fig. 2 Real-time dynamics of cell coupling mediated by F-actin under electrical field stimulation in a NOI system. (a) Side-view of the graphene electric field stimulator (GEFS) showing plated neural cells. (b) An illustration of the cell-coupling mechanism between neurons. To induce cell coupling, a weak electrical field (4.5 mV/mm) was applied, and the field-of-view (FOV) was observed in real time. (c) Time-lapse images of field-induced cell interactions at 1-min intervals. The arrows demonstrate the early appearance of F-actin fibers at the onset of cellular contact. Scale bar (c)=10 μm.

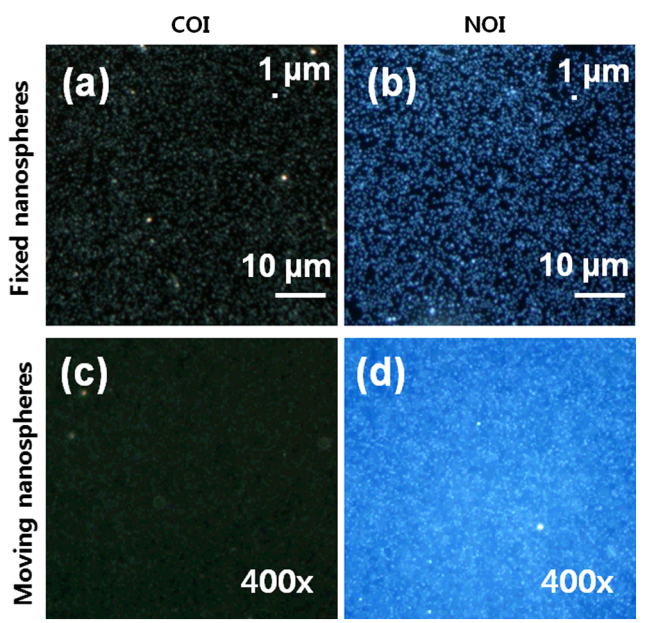

Fig. 3 Comparative images of 100 nm standard polystyrene nanospheres under COI and NOI with a high numerical aperture (NA) (1.2) dark-field condenser. Fixed: nanospheres fixed on the cover glass are visualized in dark-field view using COI (a) or NOI (b). Moving: nanospheres in the water are shown in a captured image cut from the video of either COI (c) or NOI (d).

potential as a high-resolution large FOV tool to study the fine structure and interacting behavior of the living cells.

F-actin and tubulin are the most abundant cytoskeletal proteins in neuronal cells. To identify the observed filopodial nanofibers in cells examined with the NOI system, we stained the neuronal cells with anti-F-actin, anti-tubulin antibodies (red), and 4′,6-diamidino-2-phenylindole (DAPI) (blue), and then imaged by fluorescent microscopy (FM) (Fig. 5). The nanofibers located by NOI at the cell edges correspond with the location of F-actin staining [Fig. 5(a) and 5(b)], but not with location of tubulin staining [Fig. 5(c) and 5(d)]. F-actin is a long, helical filament made of globular-actin (G-actin) subunits. These monomers are approximately 7 nm in diameter with the twist of the helix repeating every 37 nm.[33] F-actin must be observed usually after staining via FM, since the fine structure is too small to be seen by COI. In addition, these nanostructures are more difficult to image in living cells because the filament structure is dynamic.

Filopodia forms at the interacting junction of two cells (Fig. 6). Images of identical fixed and stained neural cells were used to directly compare NOI [Fig. 6(a), 6(c), and 6(e)] and FM [Fig. 6(b), 6(d), and 6(f)]. At the cell-surface edge, the protruding fine nanofibers seen using the NOI system correspond to the F-actin stained filopodial structures in the FM images [Fig. 6(c) and 6(d) to 6(e) and 6(f)]. Unstained F-actin was easily visualized by NOI because of enhanced light-scattering effects, a main

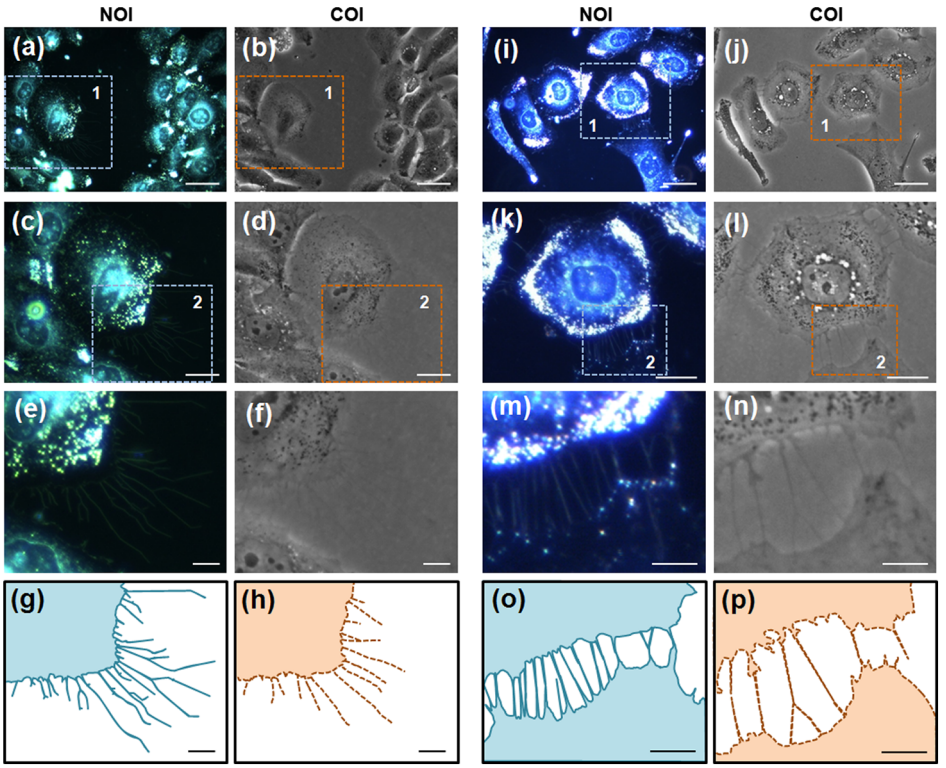

Fig. 4 Microstructures of filopodia (a)–(h) and cell junctions (i)-(p) in living cells. Filopodia, upper row: NOI (a) and COI (b) images of identical areas of filopodia at the cell edge. The dashed boxed outline indicates a region targeted for further magnification. Second row: (c) and (d) are the magnified regions of (a-1, the blue dashed box) (b-1, the red dashed box), respectively. Third row: similarly, (e) and (f) are the magnified images of (c-2) and (d-2), respectively. NOI (e) shows the microfibers more clearly than does COI (f). Cell junctions, upper row: (i) and (j) show the cell connections imaged by NOI (i) and COI (j), respectively. As before, a dashed boxed outline indicates a region targeted for further magnification. Second row: (k) is a magnified image of (i-1, the blue dashed box), and (l) is a magnified image of (j-1, the red dashed box), respectively. Third row: (m) and (n) are magnified images of (k-2) and (l-2), respectively. The microfiber connections at the junction are visible in more detail in (m) than in (n). The drawing of the cell boundary (g)–(h) and microfibers (o)–(p) show the distinct formations in morphology. Scalebars = 50 μm: (a), (b), (i), and (j); 25 μm: (c), (d), (k), and (l); and 10 μm: (e), (f), (m), and (n).

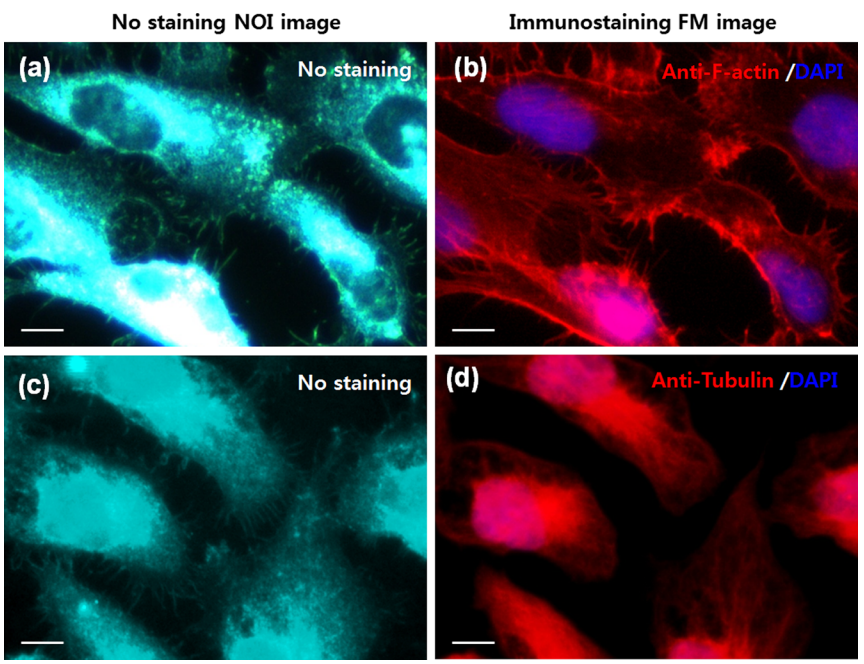

Fig. 5 Identification of nanofibers in fixed-cell images from NOI (a, c) through the comparison with FM imaging (b, d): direct comparisons are shown between (a) and (b) and (c) and (d). FM images show staining with either anti-F-actin antibody (b) or with anti-tubulin antibody (d). All scale bars = 10 μm.

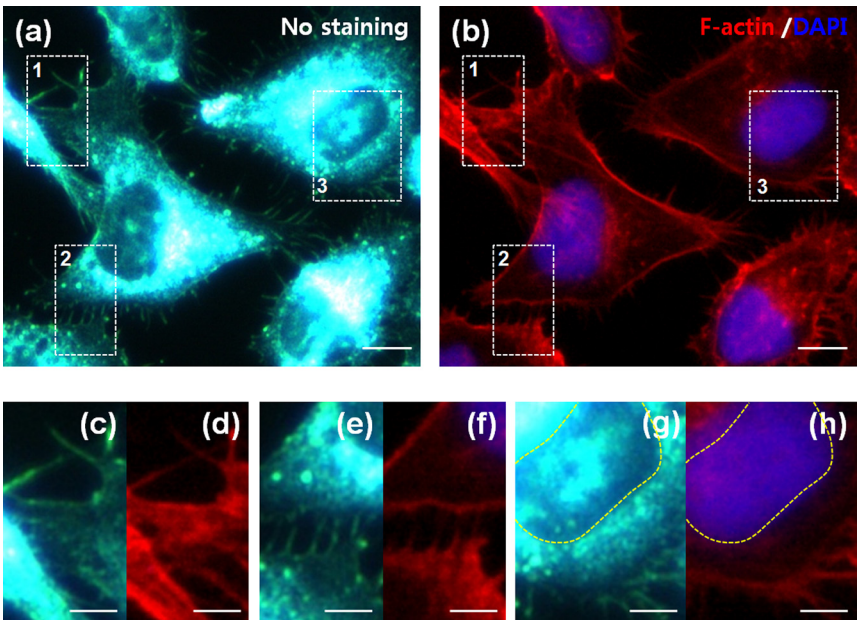

Fig. 6 Direct visualization and comparison of F-actin in the same fixed neural cells between NOI (a) and fluorescent microscopy (FM) (b). In FM, F-actin is stained red, and DNA is stained blue. The dashed boxed outlines 1, 2, or 3 indicate regions targeted for further magnification. Further comparisons of NOI and FM images are shown in (c) and (d), (e) and (f), and (g) and (h), which are magnified images of (a-1) and (b-1), (a-2) and (b-2), and (a-3) and (b-3), respectively. The yellow outline of the nucleus in the NOI image (g) is overlaid on the 4′,6-diamidino-2-phenylindole (DAPI) image in the FM image (h). Scale bars = 10 μm: (a) and (b); 5 μm : (c), (d), (e), (f), (g), and (h).

signal for dark-field imaging. The nuclear membrane was also well distinguished in NOI. In contrast, using ordinary optical imaging techniques, DAPI-stained nuclei cannot be used to view nuclear membranes because DAPI stains only the DNA. However, using NOI, unstained nuclear membranes were clearly observed [Fig. 6(g) and 6(h)].

2.3 *NOI for the Study of Stimulus-Triggered F-Actin Dynamics*

To further demonstrate the benefits of NOI for high-resolution large FOV and real-time imaging, we studied fast F-actin dynamics. In the filopodia, F-actins polymerizes to form cytoplasmic projections that are involved in cell migration, division, and differentiation, and that establish cell junctions and cell shape.[34] Previously, using a COI system for live cell imaging, a weak nEFS field (4.5 mV/m) enhanced cell coupling through more frequent cell membrane contact (lamellipodial contact).[32] Cell coupling was mediated by a vigorous generation of actin filaments, and RT-PCR showed an increase in the mRNA level of F-actin.[32]

In this study, we used NOI to observe the interactive dynamics of nEFS-enhanced cell coupling (Fig. 2). Figure 2 depicts the experimental conditions for accelerating F-actin dynamics with electrical field stimulation. First, our *in vitro* graphene electric field stimulator (GEFS) is illustrated in side view [Fig. 2(a)]. Second, the transparent ± graphene electrodes can be visualized with a phase-contrast optic image with the cells. Third, the neural cell-coupling behavior is promoted by nEFS. Finally, field-induced F-actin formation progresses via several steps, as shown in schematic [Fig. 2(b)] and in NOI real-time images [Fig. 2(c)].

The cells show a wavering behavior in the observation period before stimulation (1 to 2 min prior). For the 2 min following nEFS, early contact is formed by a few actin filaments that repeatedly make and break contact. With nEFS inducing the cells to interact more quickly and strongly, filopodial contact was enhanced first (from 3 to 4 min) followed by the lamellipodia (from 5 to 7 min). In Fig. 2, the arrows show the appearance of the F-actin nanofibers that make cellular contact. F-actin readily initiates cell coupling with the assistance of a weak electric field created by nEFS. The NOI system offers an enhanced ability to view the fast changing F-actin structure (at the nanoscale level) in unstained living cells in real time.

3 Discussion

In cell research, a conventional optical condenser (NA = 0.55) is widely used for inverted optical microscopy. So, we used a conventional type for phase-contrast images for comparison. The NOI system enhances optical resolution with its cardioid annular condenser (NA = 1.2 to 1.4).[28] To compare the resolving power of COI and NOI systems having the same NA value, we used a dark-field condenser (NA = 1.2) on a COI system to view 100 nm standard nanospheres (Fig. 3). Fixed nanospheres can be seen with COI [Fig. 3(a)], even though the structures in NOI [Fig. 3(b)] are much clearer. Likewise, mobile nanospheres were less resolved in COI [Fig. 3(c)] than in NOI [Fig. 3(d)].

During cell coupling, NOI enables observation of filopodial nanofibers [Fig. 2(b), middle], while COI limits observation to lamellipodial contact [Fig. 2(b), right]. NOI clearly shows the fine structure of F-actin fibers on the cell's leading edge [Fig. 2(c)]. Using NOI with nEFS, we were able to study the changing behavior of F-actin during cell coupling. F-actin exhibited alternating contact/release behavior for the first 2 min after stimulation. At 3-min poststimulation, the fibers were anchored tightly in filopodia leading to lamellipodial contact at 5-min poststimulation. Cell coupling was complete in the final image taken at 7-min poststimulation.

The nEFS system was developed to view the behavior of cells exposed to an electric field with an inverted microscope.[32,35]

Since it is not possible to take images using a system that contains metal electrodes, our system employs transparent graphene electrodes instead. Therefore, we can image cellular nanostructure over the electrodes and simultaneously track fast dynamics induced by stimulation of the cells. Previously, we confirmed that F-actin mRNA levels were greatly increased under nEFS.[32] In this report, finally we could use NOI with nEFS to directly examine F-actin's role in cell behavior at the point of F-actin increase.

Improvement of NOI resolution is gained by using a short-wavelength light source, such as a metal halide bulb. However, the short wavelengths include UV, which can be harmful to cells. To minimize damage, we used a green band-pass filter to protect the cells from UV light, and live cell imaging was discontinued after 1 h.

In conclusion, optical microscopy of unstained living cells can be performed with nanoscale resolution achieved by combining a conventional optical microscope with high-resolution dark-field condenser and an illumination system. With this system, we can view nanostructures like bundles of F-actin. Moreover, since NOI enables observation of unstained living cells, we can the study dynamic cellular events in real time, in our case, the F-actin changes that take place during cell coupling promoted by weak nEFS. Using NOI, we were able to see that cell coupling was initiated first by the formation of a single F-actin fiber in the filopodia, followed by cell membrane contact. This easily applicable nanoscale-resolution optical microscopy can be used in future studies to understand the various fine structural responses in cellular phenomena that require real-time observations of living cells.

4 Materials and Methods

4.1 *Nanoscale Optical Imaging*

Our NOI system was created by modifying a conventional Leica microscope (Leica Microsystems GmbH, Wetzlar, Germany) with a high-resolution dark-field condenser (CytoVivia, Inc., Auburn, Alabama) and an illuminator system (white LED and halogen light; Dolan-Jenner Industries Inc., Boxborough, Massachusetts/metal halide light; Welch Allyn Inc., Skaneateles, New York). The microscope's conventional optical condenser (NA = 0.55) was replaced by a high-resolution dark-field condenser (NA = 1.2 to 1.4). This system provides 100 nm resolution improving the contrast and signal-to-noise ratio.[28] The system's resolution was confirmed by imaging polystyrene spheres with 100 nm standard monodisperse nanospheres [Fig. 1(d); mean diameter = 97 ± 3 nm; Thermo Scientific, Inc., San Jose, California]. As shown in Fig. 1, the high-resolution dark-field condenser can be immersed in cell media. As a result, it could be positioned between 10 and 1000 μm directly above the neural cells plated in the culture dish. After each completed NOI experiment, the condenser was rinsed three times with distilled water and 70% ethanol, and then sterilized by UV for 30 min. A live-chamber system (TC-L, Chamlide, Seoul, South Korea) with a silicone top cover was used to maintain the environment at 37°C and 5% CO_2 during the experiment. Images of the living cells were recorded using a CCD camera (Leica Microsystems GmbH, Wetzlar, Germany).

4.2 *Cell Culture*

SHSY5Y human neuroblastoma cells (ATCC, Manassas, Virginia), an adhesive neural cell line, were grown in Dulbecco's modified Eagle's medium (Invitrogen, Grand Island, New York) supplemented with 10% heat-inactivated fetal bovine serum (FBS; Sigma-Aldrich, St. Louis, Missouri) and 1% penicillin-streptomycin (Invitrogen) in a T75 flask (Nunc, Thermo Fisher Scientific, Roskilde, Denmark). Cells were subcultured every three days by resuspension in 1× cell-dissociation solution (Sigma-Aldrich) with subsequent washing using 1× phosphate-buffered saline (PBS; Invitrogen). To facilitate cell attachment and growth, the neural cells were plated either on a culture dish (60 mm diameter, Techno Plastic Products AG, Trasadingen, Switzerland) or on a laminin-coated (Roche Diagnostics GmbH, Mannheim, Germany) electric field stimulator. The plated cells were maintained in a 5% CO_2 incubator (Sanyo Electric Co., Ltd., Osaka, Japan) for 24 h prior to the experiment. The cells were then examined using the COI or NOI system.

4.3 *Immunocytochemistry*

After imaging, the neural cells were fixed for 20 min with a 4% paraformaldehyde solution (Biosesang, Seongnam, South Korea) and rinsed three times with PBS at room temperature. The fixed cells were treated for 1 h with a blocking solution containing 4% normal goat serum (Vector Laboratories, Burlingame, California), 0.2% Triton X-100 (Sigma-Aldrich), 2% bovine serum albumin (Sigma-Aldrich), and 2% FBS (Sigma-Aldrich). After three 5-min PBS washes, rhodamine-conjugated phalloidin (Cytoskeleton Inc., Denver, Colorado) was applied to the cells for 1 h to stain the F-actin. For visualizing the microtubules in the cells, anti-tubulin beta3 (Millipore, Billerica Massachusetts) was applied to cells for 1 h, and then the cells were incubated in Alexa Fluor 594 (Invitrogen). After completion of the procedure for F-actin or tubulin staining, the cells were washed twice for 5 min with PBS, and then treated with DAPI (Molecular Probes, Eugene, Oregon) in PBS for 20 min to stain the nuclei. After the last 5-min PBS wash, the cells were mounted in fluorescent mounting medium (Dako Cytomation, Carpinteria, California), and then covered with a cover glass (Paul Marienfeld GmbH & Co. KG, Lauda-Königshofen, Germany).

4.4 *Graphene Electric Field Stimulator*

A transparent electric field stimulator was used to stimulate the neural cells. Procedures for manufacturing a GEFS system have been described elsewhere.[32] In this study, we modified the system by using a larger culture dish (60 mm in diameter) in order to approach the high-resolution dark-field condenser with a submicrometer closure [Fig. 2(a)]. The neural cells on a cover slide were indirectly exposed to an electric field generated by two transparent graphene electrodes (gap distance approximately 280 μm) assembled under the cover slide.

4.5 *Noncontact Electrical Field Stimulation Paradigm*

The GEFS electrodes were connected to a pulse generator. An electrical pulse was generated by a 9-channel programmable pulse stimulator (Master-9; A.M.P.I., Jerusalem, Israel) and two stimulus isolators (ISO-Flex; A.M.P.I.). Charge-balanced biphasic pulse trains with a frequency of 1 Hz and pulse width of 250 ms were applied repeatedly. The biphasic pulse trains were delivered 36 times every 100 s for 60 min. Each stimulation train was applied for 10 s at 90-s intervals for an

hour of imaging time. The electric field strength was 4.5 mV/mm, and the neural cell behavior was recorded with the optical microscope every minute. A total of 60 time-lapse imaging frames were obtained during the electrical field stimulation.

Acknowledgments

This work was supported by the Research Center Program of IBS and WCU program (R31-2008-10029) of the National Research Foundation of Korea (NRF) grant funded by the Korea government (MEST), and also by a grant of the Korean Health Technology R&D Project, Ministry of Health & Welfare, Republic of Korea (A110097).

References

1. J. J. Breunig et al., "Notch regulates cell fate and dendrite morphology of newborn neurons in the postnatal dentate gyrus," *Proc. Natl. Acad. Sci. U.S.A.* **104**(51), 20558–20563 (2007).
2. T. Q. Vu et al., "Peptide-conjugated quantum dots activate neuronal receptors and initiate downstream signaling of neurite growth," *Nano Lett.* **5**(4), 603–607 (2005).
3. C. M. Niell and S. J. Smith, "Live optical imaging of nervous system development," *Annu. Rev. Physiol.* **66**, 771–798 (2004).
4. P. M. Kulesa and S. E. Fraser, "Neural crest cell dynamics revealed by time-lapse video microscopy of whole embryo chick explant cultures," *Dev. Biol.* **204**(2), 327–344 (1998).
5. T. Misgeld et al., "Imaging axonal transport of mitochondria in vivo," *Nat. Methods* **4**(7), 559–561 (2007).
6. M. H. Histed et al., "Direct activation of sparse, distributed populations of cortical neurons by electrical microstimulation," *Neuron* **63**(4), 508–522 (2009).
7. N. Tandon et al., "Alignment and elongation of human adipose-derived stem cells in response to direct-current electrical stimulation," in *Engineering in Medicine and Biology Society, 2009. EMBC 2009. Annual International Conference of the IEEE*, Minneapolis, MN, pp. 6517–6521 (2009).
8. Y. Nazirizadeh et al., "Photonic crystal slabs for surface contrast enhancement in microscopy of transparent objects," *Opt. Express* **20**(13), 14451–14459 (2012).
9. L. Limozin and K. Sengupta, "Quantitative reflection interference contrast microscopy (RICM) in soft matter and cell adhesion," *ChemPhysChem* **10**(16), 2752–2768 (2009).
10. O. C. Rodriguez et al., "Conserved microtubule-actin interactions in cell movement and morphogenesis," *Nat. Cell Biol.* **5**(7), 599–609 (2003).
11. V. Lemmon et al., "Neurite growth on different substrates: permissive versus instructive influences and the role of adhesive strength," *J. Neurosci.* **12**(3), 818–826 (1992).
12. K. L. Briggman and W. Denk, "Towards neural circuit reconstruction with volume electron microscopy techniques," *Curr. Opin. Neurobiol.* **16**(5), 562–570 (2006).
13. A. W. Schaefer et al., "Filopodia and actin arcs guide the assembly and transport of two populations of microtubules with unique dynamic parameters in neuronal growth cones," *J. Cell Biol.* **158**(1), 139–152 (2002).
14. J. Laishram et al., "A morphological analysis of growth cones of DRG neurons combining atomic force and confocal microscopy," *J. Struct. Biol.* **168**(3), 366–377 (2009).
15. J. Rheinlaender et al., "Comparison of scanning ion conductance microscopy with atomic force microscopy for cell imaging," *Langmuir* **27**(2), 697–704 (2011).
16. D. S. Lidke and K. A. Lidke, "Advances in high-resolution imaging—techniques for three-dimensional imaging of cellular structures," *J. Cell Sci.* **125**(11), 2571–2580 (2012).
17. S. Munck et al., "Sub-diffraction imaging on standard microscopes through photobleaching microscopy with non-linear processing," *J. Cell Sci.* **125**(9), 2257–2266 (2012).
18. S. Hell and E. H. K. Stelzer, "Fundamental improvement of resolution with a 4Pi-confocal fluorescence microscope using two-photon excitation," *Opt. Commun.* **93**(5–6), 277–282 (1992).
19. S. W. Hell, "Far-field optical nanoscopy," *Science* **316**(5828), 1153–1158 (2007).
20. E. Rittweger et al., "STED microscopy reveals crystal colour centres with nanometric resolution," *Nat. Photonics* **3**, 144–147 (2009).
21. R. Schmidt et al., "Spherical nanosized focal spot unravels the interior of cells," *Nat. Methods* **5**(6), 539–544 (2008).
22. M. J. Rust et al., "Sub-diffraction-limit imaging by stochastic optical reconstruction microscopy (STORM)," *Nat. Methods* **3**(10), 793–795 (2006).
23. E. Betzig et al., "Imaging intracellular fluorescent proteins at nanometer resolution," *Science* **313**(5793), 1642–1645 (2006).
24. S. T. Hess et al., "Ultra-high resolution imaging by fluorescence photoactivation localization microscopy," *Biophys. J.* **91**(11), 4258–4272 (2006).
25. C. Yang et al., "Novel roles of formin mDia2 in lamellipodia and filopodia formation in motile cells," *PLoS Biol.* **5**(11), e317 (2007).
26. R. A. Hoebe et al., "Controlled light-exposure microscopy reduces photobleaching and phototoxicity in fluorescence live-cell imaging," *Nat. Biotechnol.* **25**(2), 249–253 (2007).
27. S. A. Jones et al., "Fast, three-dimensional super-resolution imaging of live cells," *Nat. Methods* **8**(6), 499–508 (2011).
28. A. Vainrub et al., "Resolution of 90 nm (lambda/5) in an optical transmission microscope with an annular condenser," *Opt. Lett.* **31**(19), 2855–2857 (2006).
29. A. Nair et al., "Enhanced intratumoral uptake of quantum dots concealed within hydrogel nanoparticles," *Nanotechnology* **19**(48), 485102 (2008).
30. J. N. Meyer et al., "Intracellular uptake and associated toxicity of silver nanoparticles in Caenorhabditis elegans," *Aquat. Toxicol.* **100**(2), 140–150 (2010).
31. K. Sarlo et al., "Tissue distribution of 20 nm, 100 nm and 1000 nm fluorescent polystyrene latex nanospheres following acute systemic or acute and repeat airway exposure in the rat," *Toxicology* **263**(2–3), 117–126 (2009).
32. C. Heo et al., "The control of neural cell-to-cell interactions through non-contact electrical field stimulation using graphene electrodes," *Biomaterials* **32**(1), 19–27 (2011).
33. A. Berepiki et al., "Actin organization and dynamics in filamentous fungi," *Nat. Rev. Microbiol.* **9**(12), 876–887 (2011).
34. F. Korobova and T. Svitkina, "Arp2/3 complex is important for filopodia formation, growth cone motility, and neuritogenesis in neuronal cells," *Mol. Biol. Cell* **19**(4), 1561–1574 (2008).
35. C. Heo et al., "Enhanced mobility of neural cells with a transparent electric field stimulator," *J. Nanosci. Nanotechnol.* **12**(7), 5222–5227 (2012).